uncertainty of the measured velocity dispersions. Being more conservative, in column 8 of Table 6, we derived the final error of the measured σ as the quadratic combination of both uncertainties (columns 10 and 11). These values are used for further analysis in this paper and Paper II (Kourkchi et al. 2012).

We performed the same analysis to obtain the uncertainty of the measured radial velocities. The effect of the template mismatch on measured radial velocities is less than 1 per cent, because this measurement is only sensitive to the exact location of the absorption lines of the applied stellar templates which are slightly altered from one template to another. The final radial velocities and their corresponding uncertainties are obtained based on the Set80 run (columns 5 and 6 of Table 6).

5 RESULTS AND DISCUSSION

We present the radial velocities, V_r, and velocity dispersions, σ, of 41 dwarf elliptical galaxies in the Coma cluster in Table 6. Of these galaxies, 12 have S/N $<$ 15 pixel^{-1} in their spectra. The reported values are measured based on Set80, as explained in Section 3.

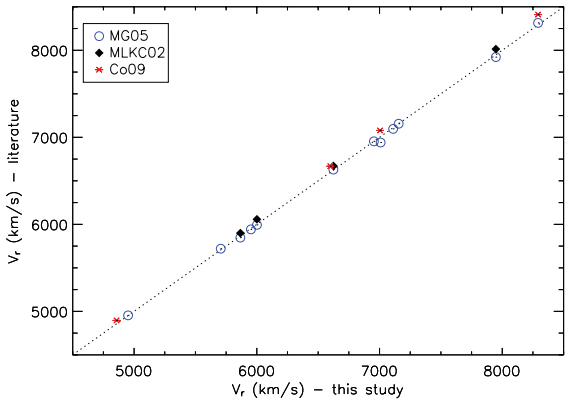

Figure 9. Radial velocities from MG05 (open circles), MLKC02 (filled diamonds) and Co09 (red stars) versus velocities in this study. The dotted line shows equality indicating that the velocities of MLKC02 and Co09 are systematically greater.

We compare our measured V_r and σ values with MG05, MLKC02 and Co09 in Figs 9 and 10. The mean difference between our V_r values and those of MG05 is $\sim$8 km s^{-1}. However, when we include the V_r measurements from Co09, the mean difference is $\sim$20 km s^{-1}. Comparison of the velocity dispersion with MG05 (see Fig. 10) shows that for smaller values of velocity dispersion (i.e. $\sigma < 50$ km s^{-1}), our values are relatively smaller. Such discrepancy is likely due to the different methods of measurement, and/or to different templates used for measurement and/or to different wavelength regimes used for analysis. Since CaT lines are more prominent in dE galaxies than the absorption lines in the wavelength range $\sim$4200–5700 Å, as used in the studies of MG05 and Co09, our measurements of V_r and σ are more robust. Our analysis also includes measurements with 80 mixed stellar templates and detailed analysis of the uncertainties.

In addition, of 41 studied galaxies in this paper, 12 galaxies were observed twice using two different masks. In Table 7, for each

Table 7. The measured velocity dispersion of the galaxies which were observed with two different masks. Columns 2 to 5 are the mask IDs also presented in Table 1. For these galaxies, we added both spectra of two masks to get the larger S/N values. In the last column, the measured velocity dispersion of the added spectra is presented. The velocity dispersions are in terms of km s^{-1} and the errors are based on the statistical uncertainties. As seen, the measured velocity dispersions for each galaxy are consistent within the error bars.

GMP	Coma1-1	Coma1-2	Coma2-1	Coma2-2	Add
3424	–	–	27 ± 7	26 ± 7	27 ± 5
3223	16 ± 9	29 ± 8	–	–	22 ± 5
3209	32 ± 3	29 ± 5	–	–	30 ± 2
3119	40 ± 7	32 ± 7	–	–	37 ± 5
3080	–	–	8 ± 9	13 ± 9	9 ± 5
2983	23 ± 6	28 ± 5	–	–	27 ± 3
2877	–	–	32 ± 8	30 ± 7	29 ± 5
2808	–	–	75 ± 11	71 ± 9	69 ± 8
2755	22 ± 6	31 ± 7	–	–	27 ± 4
2718	–	–	33 ± 5	29 ± 6	30 ± 4
2605	41 ± 9	32 ± 8	–	–	36 ± 6
2571	–	–	17 ± 4	14 ± 4	17 ± 3

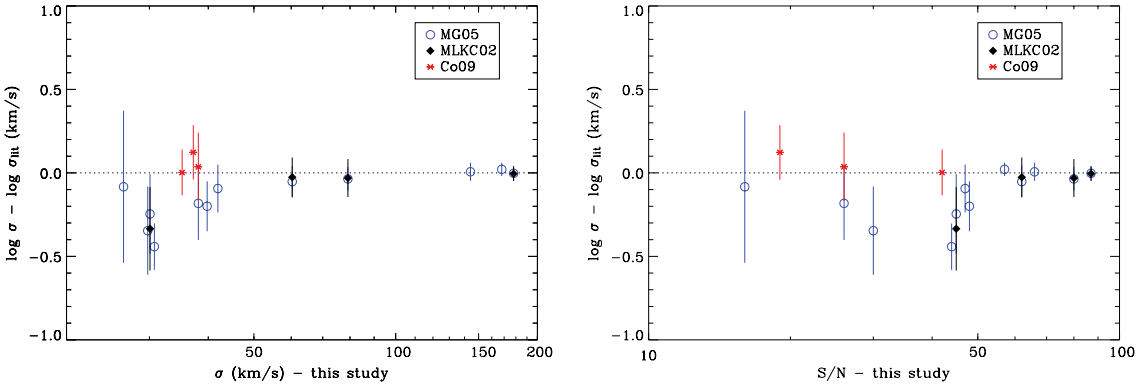

(a) (b)

Figure 10. The differences in measured velocity dispersion in this study and common galaxies in the literature (MG05, MLKC02 and Co09) are plotted against our measured velocity dispersion and S/N value in the left- and right-hand panels, respectively. To derive 1σ errors, the errors of our σ measurement and those from the literature are added in quadrature. The horizontal axis is logarithmically scaled. As seen, except for four measured values, the rest are consistent with the literature within the error bars. There is a good consistency for $\sigma > 50$ km s^{-1} for which $\langle\sigma/\sigma_{\rm lit}\rangle$ is 0.97 ± 0.05 and for $\sigma < 50$ km s^{-1} for which $\langle\sigma/\sigma_{\rm lit}\rangle$ is 0.97 ± 0.17.

of these galaxies we compare the measured velocity dispersions using both observed spectra. We also added both spectra of these galaxies to get better S/N and then repeated the measurements. As seen, considering the statistical uncertainties, the measurements are consistent.

5.1 Faber–Jackson relation

The relation between luminosity and velocity dispersion of bright elliptical galaxies was originally discovered by Faber & Jackson (1976) and is expressed as $L \propto \sigma^{\alpha}$. For brighter ellipticals α is $\sim$4 while fainter galaxies exhibit a shallower slope. Davies et al. (1983) were the first to note that α changes from $\sim$4 to $\sim$2.4, for elliptical galaxies fainter than $M_R \simeq 21.7$ mag. This result was also confirmed by Held et al. (1992) who found $\alpha = 2.5$ for dE galaxies. These results were finally extended to lower luminosities by MG05 and Co09 who found $\alpha \simeq 2.0$. In this paper, we present data for 26 dE galaxies in the Coma cluster down to $M_R \simeq -15$ mag. Using the orthogonal distance regression, we derive the FJ relation to be $L \propto \sigma^{2.34\pm0.19}$ for the entire sample, and $L \propto \sigma^{1.99\pm0.14}$ for galaxies brighter than $M_R \simeq -16$ mag.

We show the L–σ relation for the galaxies in our sample in Figs 11 and 12, where we also include the sample of Co09 and MG05. We excluded the spiral galaxies from Co09 when deriving the FJ relation. The L–σ correlation coefficient is -83 per cent at a significance of 99.99 per cent (i.e. only a 0.01 per cent chance that the correlation is due to the random scatter). We perform linear fits via two methods, the least-squares bisector fit and the orthogonal distance regression. Both methods incorporate the errors in our measurements and those reported in the literature. In orthogonal distance regression, the orthogonal distance of data points from the line is minimized. The magnitudes of all galaxies in Fig. 11 and the left-hand panel of Fig. 12 are derived from SDSS DR7. To transform SDSS *ugriz* magnitudes into the Johnson–Cousins

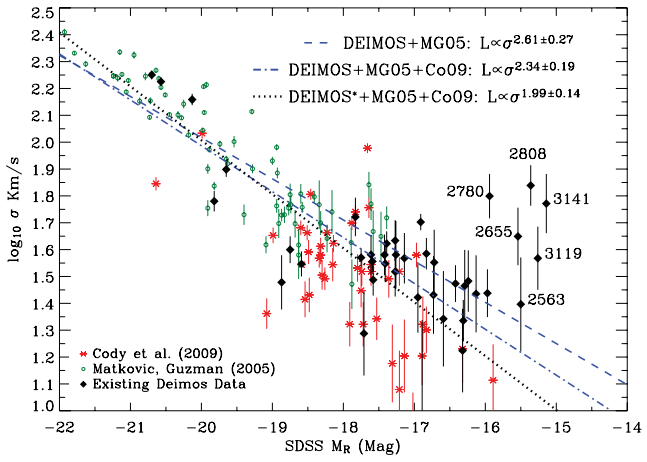

Figure 11. The FJ relation for three samples of dwarf galaxies in the Coma cluster. The filled black diamonds represent the dwarf elliptical sample from DEIMOS/Keck observations. The red asterisks are dEs from C09 and the green open circles are data from MG05. Except for one point, the DEIMOS sample provides the only measurements at $M_R \geq -16$. The dashed line is the least-squares orthogonal distance fit for DEIMOS+MG05 data while the dash–dotted line is the best orthogonal fit for all three samples. Of our sample, six of the faintest galaxies are labelled with their GMP IDs. The dotted line shows the least-squares orthogonal fit excluding the six galaxies fainter than $M_R = -16$ mag. See Table 8 for detailed results.

R magnitude, we used the mean value of the following relations presented on the SDSS DR6 website.[2]

$$R = r - 0.1837 \times (g - r) - 0.0971, \quad (3)$$

$$R = r - 0.2936 \times (r - i) - 0.1439. \quad (4)$$

The results of the least-squares fit are available in Table 8. We ran the same analysis for the same sample using the Canada–France–Hawaii Telescope (CFHT) Megacam i-band data. We find that our FJ relation slope is consistent with those of Co09 and MG05 within the errors, for both linear fitting methods. The least-squares bisector method yields $L_R \propto \sigma^{1.94\pm0.16}$, while we derive $L_R \propto \sigma^{2.34\pm0.19}$ via the orthogonal regression method. Using the CFHT i-band data, the best fits of the FJ relation are consistent with those derived from SDSS data (see Table 8). The behaviour at the faint end of the FJ relation is uncertain as many of our galaxies in this magnitude range ($M_R > -16$) have S/N < 15 pixel^{-1}. However, our results imply that the slope of the FJ relation may change towards higher velocity dispersions at this faint end. Excluding galaxies fainter than $M_R \simeq -16$, FJ is $L_R \propto \sigma^{1.99\pm0.14}$.

Next, we use photometry from the *HST*/ACS Coma Treasury Survey (Carter et al. 2008) to derive the FJ relation. Out of 41 galaxies in our sample, 28 have available *HST*/ACS magnitudes, together with 43 galaxies from the MG05 and Co09 samples. In Fig. 12 and Table 8, we show the best linear fits of the FJ relation using *HST*/ACS *F814W* (I band) and *F475W* (g band). We find that the FJ relation shows no discrepancy in colour.

Following all the above analysis, we noted that for one of our sample galaxies (GMP 3308), the SDSS magnitudes are almost one magnitude fainter than what is derived from CFHT and *HST* images. Therefore, we modified the SDSS R magnitude of this galaxy by constructing a linear trend between the CFHT i band and SDSS R magnitudes of all sample galaxies.

5.2 Colour–σ relation

The relation between the dynamical mass of galaxies and their stellar population can be studied using the colour–σ diagram. MG05 showed a well-defined colour–σ relation for faint early-type galaxies brighter than $M_R = -17.5$ mag. In panel (A) of Fig. 13, we extend the relation to fainter dEs ($M_R < -15$ mag) which are located at the blue end of the diagram and are more scattered around the the fitted line for brighter galaxies [i.e. for $M_R > -17$ mag the relation is $B - R = (0.23 \pm 0.03) \log \sigma + (1.02 \pm 0.23)$]. The scatter of dEs around the colour–σ relation could be due to their different formation history, age and metallicity. To calculate the colour of the galaxies, $B - R$, we used the SDSS data and the transformation functions presented on the SDSS website to derive the Johnson B and R magnitudes. Panel (B) of Fig. 13 shows the same relation using $m_{475} - m_{814}$ colour of the galaxies in the *HST*/ACS field.

The dependence of the internal velocity dispersion of dEs and their central activity is investigated in panel (C) of Fig. 13. Central colours of the galaxies for which we have the *HST*/ACS images are calculated within the aperture with a diameter of 0.4 arcsec (i.e. 185 pc at the location of the Coma cluster). We found a linear trend between the velocity dispersion of dEs and their central colours, except for very faint galaxies which have bluer cores, $(m_{475} - m_{814}) < 1.0$.

[2] http://www.sdss.org/dr6/algorithms/sdssUBVRITransform.html, see also Jordi, Grebel & Ammon (2006) and Ivezić et al. (2007).

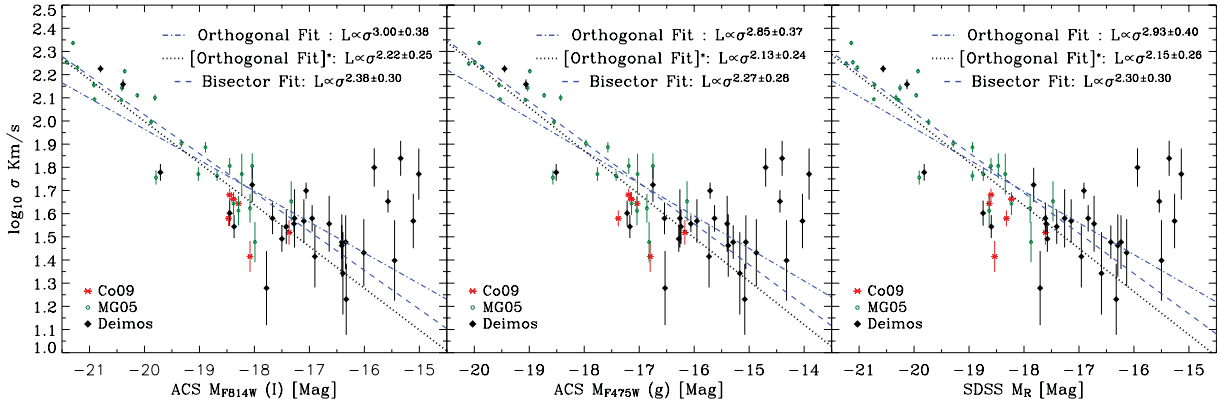

Figure 12. Same as Fig. 11. The FJ relation for three samples of dwarf galaxies which lie in the footprint of the *HST*/ACS Coma Treasury Survey (Carter et al. 2008). The left-hand panel shows the FJ relation for this sample using magnitudes based on SDSS data. For the left-hand and middle panels, magnitudes are derived from the Treasury *HST*/ACS images in the *F814W* (*I* band) and *F475W* (*g*-band) filters (Paper II). The dashed line is the least-squares bisector fit, and the dash–dotted line is obtained using the orthogonal distance regression. The dotted line shows the orthogonal fit for galaxies brighter than $M_R = -16$ mag. We see no colour dependence of the FJ within the error bars.

Table 8. Least-squares fit to find the L–σ relation. (1) The sample galaxies used in regression. (2) Survey filters for the magnitude of the sample galaxies. (3) The order of regression. For example, in the first row residuals in $\log\sigma$ are minimized. (4) and (5) The slope and intercept of $M = A\log\sigma + B$ and their 1σ uncertainties. (6) α in the FJ relation ($L \propto \sigma^{\alpha}$). We have used the data with S/N > 15 Å^{-1} of MG05 and all dEs of Co09.

Sample galaxies (1)	Filter (2)	Regression (3)	Slope (A) (4)	Intercept (B) (5)	α (6)
DEIMOS+MG05	SDSS *R*	$\log\sigma$	-6.59 ± 0.67	-6.72 ± 2.17	2.64 ± 0.27
DEIMOS+MG05	SDSS *R*	M_R	-4.55 ± 0.38	-10.45 ± 0.76	1.81 ± 0.15
DEIMOS+MG05	SDSS *R*	Bisector	-5.57 ± 0.55	-8.59 ± 1.63	2.23 ± 0.22
DEIMOS+MG05	SDSS *R*	Orthogonal	-6.52 ± 0.67	-6.84 ± 2.19	2.61 ± 0.27
DEIMOS*+MG05	SDSS *R*	Orthogonal	-5.41 ± 0.49	-9.02 ± 2.02	2.16 ± 0.20
DEIMOS+MG05+Co09	SDSS *R*	Bisector	-4.85 ± 0.40	-10.12 ± 1.31	1.94 ± 0.16
DEIMOS+MG05+Co09	SDSS *R*	Orthogonal	-5.85 ± 0.49	-8.37 ± 1.79	2.34 ± 0.19
DEIMOS*+MG05+Co09	SDSS *R*	Orthogonal	-4.98 ± 0.35	-10.00 ± 1.58	1.99 ± 0.14
DEIMOS+MG05+Co09	CFHTLS *i*	Bisector	-4.73 ± 0.38	-10.33 ± 1.27	1.89 ± 0.15
DEIMOS+MG05+Co09	CFHTLS *i*	Orthogonal	-5.61 ± 0.45	-8.81 ± 1.73	2.25 ± 0.18
DEIMOS*+MG05+Co09	CFHTLS *i*	Orthogonal	-4.82 ± 0.33	-10.29 ± 1.54	1.93 ± 0.13
[DEIMOS*+MG05+Co09]	*HST*/ACS *F814W* (*I*)	Orthogonal	-5.55 ± 0.63	-8.90 ± 2.49	2.22 ± 0.25
[DEIMOS*+MG05+Co09]	*HST*/ACS *F475W* (*g*)	Orthogonal	-5.33 ± 0.61	-8.02 ± 2.35	2.13 ± 0.24
[DEIMOS*+MG05+Co09]	SDSS *R*	Orthogonal	-5.37 ± 0.64	-9.21 ± 2.64	2.15 ± 0.26

All galaxies in the [DEIMOS+MG05+Co09] sample have *HST*/ACS data. DEIMOS* represents the DEIMOS sample excluding galaxies fainter than $M_R = -16$ mag.

5.3 Remarks on faint galaxies

Of six faintest galaxies from the DEIMOS sample, GMP 2808, GMP 2655, GMP 3119, GMP 2780 and GMP 3141 are bluer than all other sample galaxies (see Fig. 13) and have larger velocity dispersion with respect to the L–σ relation of brighter galaxies (see Fig. 8).

In order to test the effect of stellar population on measured velocity dispersions, we have repeated the σ measurement using two sets of stellar templates. The first set consists of 10 F stars with different spectral types and metallicities (hereafter F-lib). The second set includes both F-lib and the G/K stars of Table 3 (hereafter FGK-lib). The results of σ measurements based on Set80, FGK-lib and F-lib are compared in Table 9. The analysis based on FGK-lib shows no changes in results except for GMP 2808 which is the bluest galaxy in our sample. The measured σ of GMP 3119 and GMP 2808 in the F-lib run is smaller than those of the Set80 and FGK-lib runs; however, the resulting χ^2 is higher for the F-lib run. The maximum change in measured σ for all other galaxies in our sample in the FGK-lib run is less than 2 km s^{-1}. As a result, the measured σ values in Table 6 are independent of the stellar population except for the bluest galaxy, for which blue stellar templates should be used for σ measurement.

Recent gas-rich mergers in blue dEs may be responsible for their deviation from the FJ relation. Supernova-driven winds can expel the luminous matter of these galaxies and shift them to the faint end of the FJ diagram. Moreover, the resulting starburst due to the inward gas transportation during the merger produces the central excess light compared to the extrapolated Sérsic function of the galaxy's outer region (Kormendy et al. 2009). The correlation between the central extra light and deviation of faint dEs from the scaling relations of brighter ellipticals is studied in Paper II.

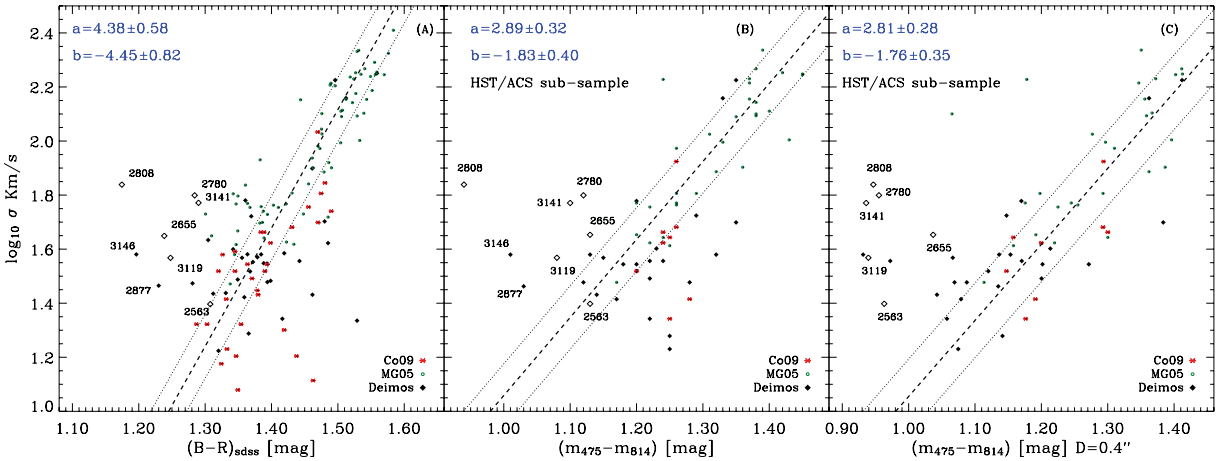

Figure 13. Colour–σ relation for three samples of dwarf ellipticals in the Coma cluster. The filled black diamonds represent dEs from our DEIMOS/Keck sample. The open diamonds represent faintest dEs of our sample which are labelled with their GMP IDs. The red asterisks are dEs from Co09 and the green open circles are from MG05. The dashed line shows the best linear orthogonal fit for brighter galaxies, $M_R > -17$ mag, and the dash–dotted lines represent 1σ uncertainty along the vertical axis. In all panels, a and b are the slope and intercept of the fitted lines, respectively. Panel (A) shows the colour–σ relation using the magnitudes from SDSS DR7. Panel (B) shows the colour−σ relation for a subsample of dEs for which their *HST*/ACS magnitudes in *F475W* (g) and *F814W* (I) bands are available. Panel (C) is the same as panel (B) except for the colour of galaxies which are calculated within the aperture with diameter of 0.4 arcsec (i.e. 185 pc at the location of the Coma cluster).

Table 9. The results of σ measurements for eight blue galaxies based on different template libraries.

GMP ID	σ (km s^{-1}) Set80	FGK-lib	F-lib
3146	38	37	35
3141	59	60	61
3119	37	35	26
2877	29	27	26
2808	69	39	38
2780	63	63	31
2655	45	45	42
2563	25	25	28

6 SUMMARY

We have observed a sample of ∼50 dwarf elliptical galaxies in the core of the Coma cluster of which we measured the internal velocity dispersions for 41 dwarfs. For 26 galaxies, we presented the velocity dispersion for the first time. Our current study extends the relation 1 mag fainter than previous studies in Coma. We performed a comprehensive analysis to find the source of the uncertainties when measuring the velocity dispersion. We found that the main uncertainty may arise due to the mismatch of the stellar templates. This kind of uncertainty is less than 20 per cent of the measured velocity dispersion for $\sigma \sim 50\,\mathrm{km\,s^{-1}}$. The template mismatch uncertainty decreases for higher velocity dispersions and is reduced to ∼5 per cent for $\sigma \gtrsim 100\,\mathrm{km\,s^{-1}}$. We find greater velocity dispersions when using templates with lower stellar metallicities. The effect of template mismatch is reduced with the use of multiple stellar templates and the optimization of the template weights to reproduce each sample galaxy spectrum. In addition, using the multiple stellar templates removes the dependence of the measurements on galaxy and/or templates metallicity. Casting our data points and those from the literature, we get the L–σ relation as $L \propto \sigma^{1.99\pm0.14}$. We noted that fainter dwarfs show a departure from the FJ relation of the brighter ellipticals, which indicates that they have a higher velocity dispersion than what is predicted by the L–σ linear trend. In Paper II, we will present the combined study of the photometric and spectroscopic properties of this sample, focusing on the Fundamental and the Photometric Plane of the galaxies.

ACKNOWLEDGMENTS

The authors wish to recognize and acknowledge the very significant cultural role and reverence that the summit of Mauna Kea has always had within the indigenous Hawaiian community. We are most fortunate to have the opportunity to conduct observations from this mountain. DC and AMK acknowledge support from the Science and Technology Facilities Council, under grant PP/E/001149/1. EM-Q acknowledges support from the SMES for a FPI PhD fellowship through the research project AYA2007-67752-C03-01. EK would like to thank Paul Westoby and Michele Cappelari for their helpful comments on running PPXF. EK also acknowledges financial support from Sharif University of Technology. This research also used the facilities of the Canadian Astronomy Data Centre operated by the National Research Council of Canada with the support of the Canadian Space Agency.

REFERENCES

Aaronson M., 1983, ApJ, 266, L11
Adami C. et al., 2006, A&A, 451, 1159
Bender R., Burstein D., Faber S. M., 1992, ApJ, 399, 462
Cappellari M., Emsellem E., 2004, PASP, 116, 138
Carrera R., Gallart C., Pancino E., Zinn R., 2007, AJ, 134, 298
Carter D. et al., 2008, ApJS, 176, 424
Cenarro A. J., Gorgas J., Vazdekis A., Cardiel N., Peletier R. F., 2003, MNRAS, 339, 12
Cody A. M., Carter D., Bridges T. J., Mobasher B., Poggianti B. M., 2009, MNRAS, 396, 1647 (Co09)
Davies R. L., Efstathiou G., Fall M., Illingworth G., Schechter R. L., 1983, AJ, 266, 41
Davis M. et al., 2003, in Guhathakurta P., ed., Proc. SPIE Vol. 4834, Discoveries and Research Prospects from 6- to 10-Meter-Class Telescopes II. SPIE, Bellingham, p. 161

De Rijcke S., Prugniel P., Simien F., Dejonghe H., 2006, MNRAS, 369, 1321
Dekel A., Silk J., 1986, ApJ, 303, 39
Díaz A. I., Terlevich E., Terlevich R., 1989, MNRAS, 239, 325
Djorgovski S., Davis M., 1987, ApJ, 313, 59
Dressler A., Lynden Bell D., Burstein D., Davies R. L., Faber S. M., Terlevich R., Wegner G., 1987, ApJ, 313, 42
Faber S. M., Jackson R. E., 1976, ApJ, 204, 668
Faber S. M. et al., 2003, in Iye M., Moorwood F. M., eds, Proc. SPIE Vol. 4841, Instrument Design and Performance for Optical/Infrared Ground-Based Telescopes. SPIE, Bellingham, p. 1657
Foster C., Forbes D. A., Proctor R. N., Strader J., Brodie J. P., Spitler L. R., 2010, AJ, 139, 1566
Geha M., Guhathakurta P., van der Marel R. P., 2002, AJ, 124, 3073
Godwin J. G., Metcalfe N., Peach J. V., 1983, MNRAS, 202, 113
Graham A. W., Guzmán R., 2003, AJ, 125, 2936
Held E. V., de Zeeuw T., Mould J., Picard A., 1992, AJ, 103, 851
Ivezić Ž. et al., 2007, in Sterken C., ed., ASP Conf. Ser. Vol. 364, The Future of Photometric, Spectrophotometric and Polarimetric Standardization. Astron. Soc. Pac., San Francisco, p. 165
Jordi K., Grebel E. K., Ammon K., 2006, A&A, 460, 339
Jørgensen U. G., Carlsson M., Johnson H. R., 1992, A&A, 254, 258
Jørgensen I., Franx M., Kjaergaard P., 1996, MNRAS, 280, 167
Kormendy J., Fisher D. B., Cornell M. E., Bender R., 2009, ApJS, 182, 216
Kourkchi E., Khosroshahi H. G., Carter D., Mobasher B., 2012, MNRAS, in press (doi:10.1111/j.1365-2966.2011.19980.x)
Lejeune Th., Cuisinier F., Buser R., 1997, A&AS, 125, 229
Mallik S. V., 1994, A&AS, 103, 279
Mateo M., 1998, ARA&A, 36, 435
Matković A., Guzmán R., 2005, MNRAS, 362, 289 (MG05)
Michielsen D. et al., 2007, ApJ, 670, 101
Moore S. A. W., Lucey J. R., Kuntschner H., Colless M., 2002, MNRAS, 336, 382 (MLKC02)
Pritchet C., 1978, ApJ, 221, 507
Schulz J., Fritze-v. Alvensleben U., Móller C. S., Fricke K. J., 2002, A&A, 392, 1
Smith G., Drake J. J., 1990, A&A, 231, 125
Starkenburg E. et al., 2010, A&A, 513, A34
Toloba E., Boselli A., Cenarro A. J., Peletier R. F., Gorgas J., Gil de Paz A., Muñoz-Mateos J. C., 2011, A&A, 526, 114
Tonry J., Davis M., 1979, AJ, 84, 1511
Valdes F., Gupta R., Rose J. A., Singh H. P., Bell D. J., 2004, ApJS, 152, 251
Yoshii Y., Arimoto N., 1987, A&A, 188, 13
Zhou X., 1991, A&A, 248, 367

This paper has been typeset from a TEX/LATEX file prepared by the author.